Supplementary information for:

Counting RAD51 proteins disassembling from nucleoprotein filaments under tension

Joost van Mameren[1,†], Mauro Modesti[2,3], Roland Kanaar[2,4], Claire Wyman[2,4], Erwin J. G. Peterman[1,*], and Gijs J. L. Wuite[1,*]

[1] Laser Centre and Department of Physics and Astronomy, Vrije Universiteit, De Boelelaan 1081, 1081 HV, Amsterdam, The Netherlands;
[2] Department of Cell Biology and Genetics, Erasmus MC, PO Box 2040, 3000 CA Rotterdam, The Netherlands;
[3] CNRS, Unité Propre de Recherche 3081, Genome Instability and Carcinogenesis Conventionné par l'Université d'Aix-Marseille 2, 13402 Marseille Cedex 20, France;
[4] Department of Radiation Oncology, Erasmus MC, PO Box 2040, 3000 CA Rotterdam, The Netherlands.

* These authors contributed equally to this work.

[†] Present address: JPK Instruments AG, Bouchéstrasse 12, 12435 Berlin, Germany.

Supplementary Methods

Dual trap and fluorescence microscope

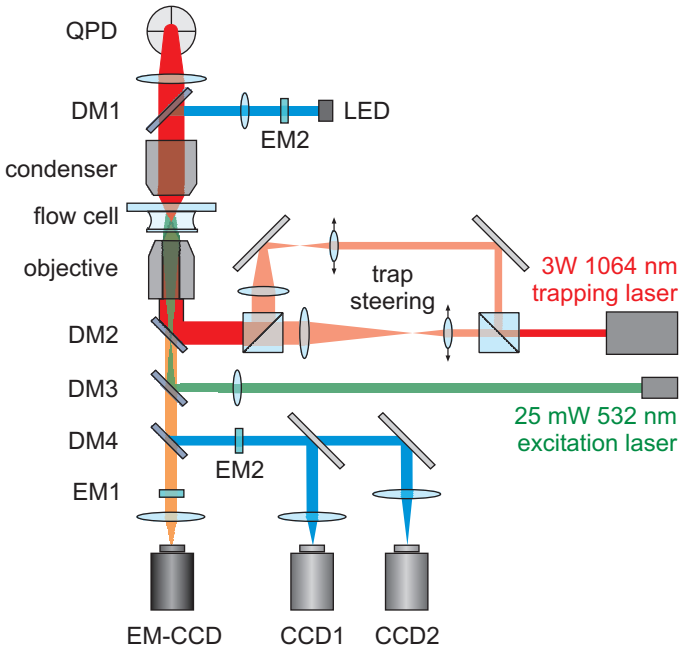

Supplementary Figure S1: Experimental apparatus. Schematic of the combined dual trap and fluorescence microscope. Abbreviations: DM – dichroic mirror; EM – emission filter; QPD – quadrant photodiode; LED – light emitting diode; (EM-)CCD – (electron-multiplied) charge coupled device. See text for details.

The combined fluorescence and optical trapping instrument was built around an Eclipse TE2000-U inverted microscope (Nikon), equipped with a stage riser kit (T-BSUK, Nikon) that allows for stacking two dichroic filter turrets. The optical traps are generated by a Nd:YVO_4 laser (Ventus 1064 nm, 3W cw, Laser Quantum, Cheshire, UK), isolated against back reflections by a Faraday isolator (IO-5-λ-HP, Optics For Research, Caldwell, NJ). This laser beam was split into two beams by a polarizing beam splitter cube (10BC16PC.9, Newport, Irvine, CA). In both beam paths, a 1 : 2.67 telescope system was implemented allowing for simultaneous beam expansion and beam steering in the sample. In one path, the first telescope lens could be displaced laterally using two computer-controlled actuators (T-LA28, Zaber Technologies Inc., Richmond, BC, Canada) to allow positioning of that trap with a joystick. The beams are recombined using a beam splitter cube and coupled via a dichroic mirror ('DM2':

950dcsp, Chroma Tech Corp., Rockingham, VT) into a water-immersion objective (Plan Apochromat 60x, NA = 1.20, Nikon) to generate the laser traps. For displacement detection of the static trap, the intensity profile in the back focal plane of the condenser (Achromat/Aplanat, NA = 1.4, Nikon) was imaged onto a quadrant photodiode ('QPD', SPOT-9DMI, UDT Sensors, Hawthorne, CA)[31]. The photocurrents from the quadrants were differentially amplified with custom electronics[31,32] to yield x and y displacement signals that were recorded using a 24 bit A/D converter (NI-PCI-4474, National Instruments). Displacement signals were calibrated using power spectrum analysis[33].

For fluorescence excitation, a 532 nm laser (GCL-025-L, 25 mW cw, Crystalaser, Reno, NV) was decollimated for widefield excitation and coupled into the second dichroic filter turret ('DM3': z532rdc, Chroma). Fluorescence emission was band-pass filtered ('EM1': hq575/50m, Chroma) and imaged onto a sensitive electron multiplying CCD camera ('EM-CCD': Cascade 512B, Princeton Instruments, Monmouth Junction, NJ) and read out using the WinView software package (Princeton Instruments). Camera readout could be externally triggered using a TTL signal for time lapsed data acquisition, reducing the illumination dose and consequently photobleaching of the dyes.

In addition, a bright-field image of the trapped beads, illuminated by a blue LED (LXHL-NB98 Luxeon Star/O, LumiLeds; using Chroma filters 'DM1': 520dcrx, 'DM4': z488rdc, and 'EM2': d440/20) was imaged onto a CCD camera (902K, Watec) that was read out by a image acquisition board (PCI-1407, National Instruments) for online measurement of bead separations.

The custom-built flow cell featuring multiple parallel, laminar channels with different buffers and reaction components that can be swiftly exchanged (see Fig. 1a) has been described elsewhere[34]. All buffers were degassed and kept under nitrogen atmosphere to reduce photobleaching. As an additional measure against photobleaching, 1 mM of the reducing agent dithiotreitol (DTT) was present in all buffer solutions.

Data analysis

Kymography

Time-lapse recorded fluorescence images were analyzed using kymographs[35], generated using custom-written LabVIEW software. This was done by (i) selecting a narrow box encompassing the DNA contour in all frames, (ii) integrating the pixel values across the DNA to obtain a single line of pixels per frame, (iii) subtracting a per-frame computed

background value, and (iv) pasting these pixel lines into consecutive columns of a single image.

Determination of disassembly rates

The tension-dependent disassembly rates such as displayed in Fig. 2c are measured as the time derivatives of integrated intensity traces, divided by the instantaneous intensity to compensate for the decreasing number of proteins and filament ends available for disassembly. The red symbols in Fig. 2c correspond to directly differentiated intensity traces, box-averaged to reduce the scatter due to differentiation (error bars represent s.e.m.). The blue symbols are the analytical derivative of a phenomenological double-exponential fit to the raw intensity trace normalized by this same raw trace. Both traces are well fitted by Arrhenius' equation:

$$k(F) = \exp[-x^{\dagger}F / k_{\mathrm{B}}T],$$

yielding the same value ($x^{\dagger}$ = 0.20 ± 0.01 nm, for this RAD51–DNA complex). Averaging data for in total 9 constructs, we determined an average $x^{\dagger}$ to be 0.27 ± 0.04 nm.

Step-fitting algorithm

The Matlab routine for the automated step-fitting algorithm[36], kindly shared by Jacob Kerssemakers (currently at the Technical University of Delft), was adapted to suppress back steps. In our implementation, the routine is run with increasing numbers of fitted steps, until the first back step is detected. The optimal number of steps for each trace was obtained both by visual inspection of the fit results and by using the fit/counterfit

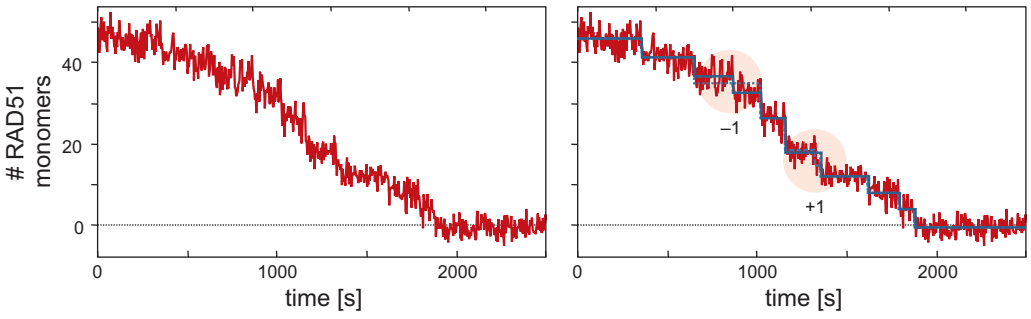

Supplementary Figure S2: Step fitting algorithm. Raw intensity trace 1 from Fig. 3a. without (left) and with (right) step fitting results. The optimal number of steps was 9 (solid blue fit); also shown are fit results with 8 and 10 steps (dashed blue lines). The segments where these changes occur are indicated by the shaded circles.

analysis as used by Kerssemakers *et al.*[36], yielding equal results. An example of a step fit with the optimal number of steps as well as one more and one less is displayed in Supplementary Fig. S2.

Fluorescence quantification

To calculate the number of RAD51 monomers from the CCD-recorded fluorescence intensity, we analyzed intensity traces of sparsely labeled RAD51-dsDNA constructs at elevated excitation powers, when photobleaching is increased. Our instrument proved capable of identifying individual bleaching steps in these traces, the size of which

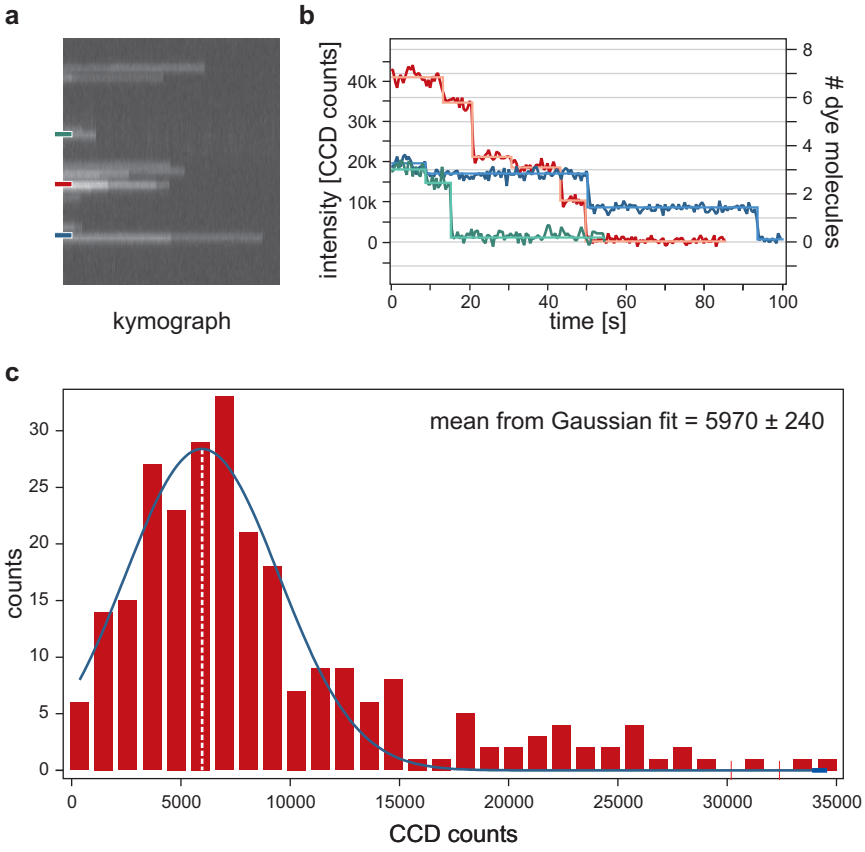

Supplementary Figure S3: Fluorescence quantification. a, Kymograph of a trapped, sparsely RAD51-coated dsDNA molecule photobleached with ~10–100× more intense excitation power than used in the disassembly studies. **b,** Intensity traces of the RAD51 patches indicated in a, indicating the stepwise bleaching. **c,** Step-size histogram of fitted bleaching steps. The Gaussian fit yields the intensity calibration.

corresponds to the fluorescence from a single Alexa Fluor 555 label (Supplementary Figs. S3a and b). We used an automated step fitting algorithm[36] to extract these steps in an unbiased manner. The distribution of step sizes and a Gaussian fit are shown in Supplementary Fig. S3c. The thus obtained intensity calibration was used to generate the right axis in Supplementary Fig. S3b.

The labeling efficiency of our RAD51 variants was determined to be 1.3 dyes per monomer using mass spectrometry[37]. We can thus calibrate the recorded intensity to the number of RAD51 monomers, trivially correcting for differences in exposure time or excitation power.

Occurrence of ATP rebinding

The characteristic burst/pause disassembly behavior as presented in Fig. 3 is also observed when the disassembling RAD51–dsDNA complexes are in a buffer containing 2 mM ATP. Fitting of the steps[36] yielded in this case an average pause duration of 97 s and thus a k_{cat} of 0.6 min^{-1} (Supplementary Fig. S4), on the same order as without ATP in the buffer solution.

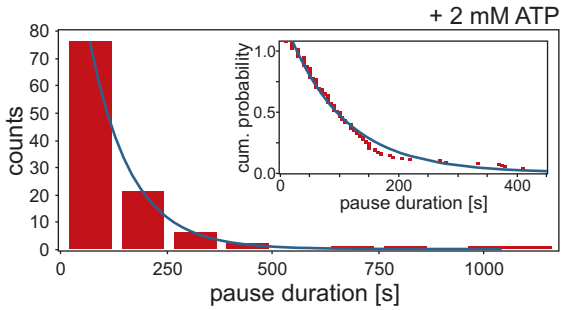

Supplementary Figure S4: Pause durations in the presence of ATP. Histogram of pause durations obtained from fitted burst/pause traces like those shown in Fig. 3, yet with the filaments disassembling in a buffer containing 2 mM ATP to check the effect of ATP renewal.

Filament length and burst size

The model described in the main text was implemented in LabVIEW-based simulations. Filaments were generated with exponentially distributed lengths (filaments with generated with identical lengths yield only minute differences), initially with ATP bound to all monomers. In an iterative manner, ATP hydrolysis was then

allowed to occur randomly along the filaments (typically with a 5‰ chance per iteration for each monomer), after which consecutive terminal monomers where ATP hydrolysis had taken place were removed.

The shape of the thus obtained disassembly traces depends on the (average) number of monomers per filament (Supplementary Fig. S5a). For long filaments, disassembly is initially limited since it only occurs from filament ends. Disassembly gradually accelerates, because the reservoir of monomers with hydrolyzed ATP grows. This growth is limited by depletion of the reservoir when filaments start to disappear entirely (end effects). For short filaments, disassembly is initially less limited due to the large relative number of ends. In addition, end effects occur sooner. By comparing

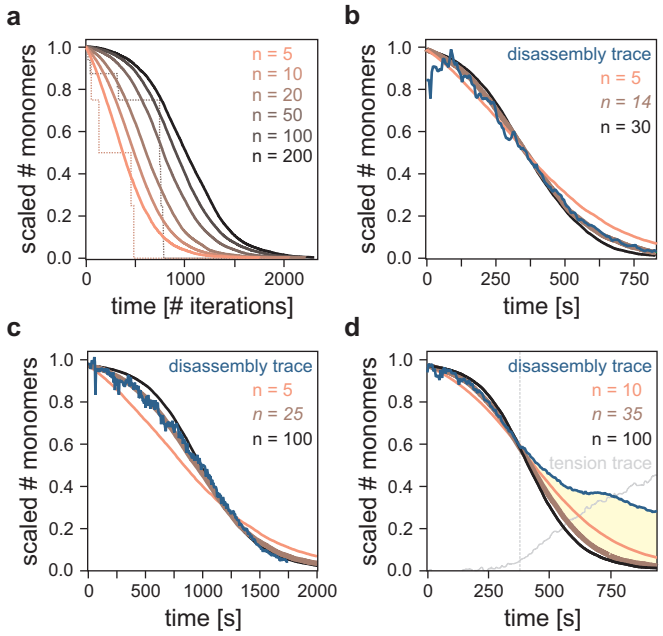

Supplementary Figure S5: Filament length. a, Simulations of our RAD51 disassembly model reveal a dependence of the shape of disassembly traces on the average initial filament length. The solid, smooth lines are averaged traces (>1000 filaments) for 6 different initial filament lengths; the dotted lines represent individual traces with 10 and 50 monomers, showing pauses and bursts of disassembly. **b–d,** This shape dependence can be exploited to estimate the average filament length in the measured disassembly traces. Filaments disassembling under small but constant DNA tension follow model traces well (panels b and c). The disassembly trace from Fig. 2a (shown here in panel d) indicates that once tension builds up (grey trace), the trace deviates from the simulated line (yellow shading), as expected. The simulated traces indicated in italic make the best fits; we obtained an average initial filament length of <50.

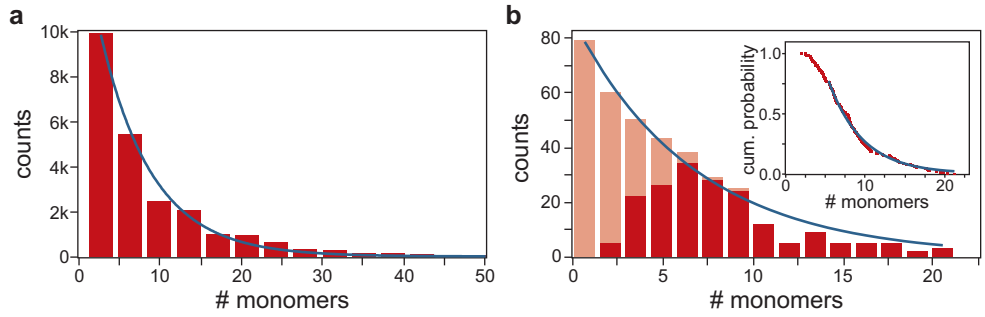

Supplementary Figure S6: Burst size distribution. a, Simulations based on the proposed model yielded exponentially distributed burst sizes, averaging to 5–10 monomers per burst for exponentially distributed initial filament lengths between 10–50 monomers. **b,** Experimentally observed burst sizes, obtained from step fits to disassembly traces, seem consistent with exponentially distributed bursts. See text for details.

these simulated traces to experimental ones, we obtained an estimate for the initial filament length in our experiments of 10-50 monomers. Disassembly traces recorded with constant DNA tension (using flow-induced drag) are well described by the model (Supplementary Figs. S5b and c). The time scales of disassembly (but not the shape) are set by the magnitude of the drag force (*cf.* Figure 2). As expected, simulated traces start to deviate once DNA tension builds up (Supplementary Fig. S5d, yellow shading). It is important to note that this relatively short filament length, similar to previous reports[37,38], depends on the experimental conditions in which filaments were assembled.

As indicated in Supplementary Fig. S6a, simulations based on the proposed model yield exponentially distributed burst sizes, averaging to 5–10 monomers per burst for exponentially distributed initial filaments lengths between 10–50 monomers.

Using the step fitting routine[36], the distribution of numbers of monomers in fitted disassembly bursts was obtained, shown as red bins in Supplementary Fig. S6b. The cumulative probability distribution (inset) suggests an exponential distribution with a mean of 5 RAD51 monomers, yet the histogram lacks small bursts (1–3 monomers), which are hidden in the noise. From the remaining average slope in fitted pause plateaus (-0.01 monomers/s; see main text), we estimate that ~1 small burst is missed per pause (~150 in total). The undetected small bursts are expected to be normally distributed with a standard deviation of 2.7 monomers (the noise in our intensity traces). The pink bins represent the 150 missed bursts that, together with the measured bursts, recover the expected exponential distribution. This consistency

further supports our model of uniform ATP hydrolysis combined with terminal RAD51 dissociation.

Supplementary Notes

31 Gittes, F & Schmidt, C. F. Interference model for back-focal-plane displacement detection in optical tweezers. *Opt Lett* **23** (1), 7-9 (1998).

32 Peterman, E. J. G., van Dijk, M. A., Kapitein, L. C., & Schmidt, C. F. Extending the bandwidth of optical-tweezers interferometry. *Rev Sci Instrum* **74** (7), 3246-3249 (2003).

33 Gittes, F. & Schmidt, C. F. Signals and noise in micromechanical measurements. *Method Cell Biol* **55**, 129-156 (1998).

34 Noom, M. C., van den Broek, B., van Mameren, J., & Wuite, G. J. L. Visualizing single DNA-bound proteins using DNA as a scanning probe. *Nat Methods* **4** (12), 1031-1036 (2007).

35 van Mameren, J. et al. Dissecting elastic heterogeneity along DNA molecules coated partly with Rad51 using concurrent fluorescence microscopy and optical tweezers. *Biophys J* **91** (8), L78-L80 (2006).

36 Kerssemakers, J. W. J. et al. Assembly dynamics of microtubules at molecular resolution. *Nature* **442** (7103), 709-712 (2006).

37 Modesti, M. et al. Fluorescent human RAD51 reveals multiple nucleation sites and filament segments tightly associated along a single DNA molecule. *Structure* **15** (5), 599 (2007).

38 van der Heijden, T. et al. Real-time assembly and disassembly of human RAD51 filaments on individual DNA molecules. *Nucleic Acids Res* **35** (17), 5646-5657 (2007).